Growth rate inhibition metrics correct for confounders in measuring sensitivity to cancer drugs

Marc Hafner[1,2], Mario Niepel[1,2], Mirra Chung[1] & Peter K Sorger[1]

Drug sensitivity and resistance are conventionally quantified by IC_{50} or E_{max} values, but these metrics are highly sensitive to the number of divisions taking place over the course of a response assay. The dependency of IC_{50} and E_{max} on division rate creates artefactual correlations between genotype and drug sensitivity, while obscuring valuable biological insights and interfering with biomarker discovery. We derive alternative small molecule drug-response metrics that are insensitive to division number. These are based on estimation of the magnitude of drug-induced growth rate inhibition (GR) using endpoint or time-course assays. We show that GR_{50} and GR_{max} are superior to conventional metrics for assessing the effects of small molecule drugs in dividing cells. Moreover, adopting GR metrics requires only modest changes in experimental protocols. We expect GR metrics to improve the study of cell signaling and growth using small molecules and biologics and to facilitate the discovery of drug-response biomarkers and the identification of drugs effective against specific patient-derived tumor cells.

The quantification of drug response is fundamental to the discovery of therapeutic molecules, the investigation of their mechanisms of action[1–3], and the study of signal transduction, cell division, and other biological processes using chemical biology approaches[4,5]. In the case of anticancer drugs, cells are typically exposed to drugs over a range of concentrations, and the number of viable cells (or surrogates, such as ATP level assayed using CellTiter-Glo, CTG) is measured several days later. Data comprising cell counts in the presence of drug divided by counts for untreated controls are fitted to a sigmoidal curve to compute (i) the concentration of drug at which the cell count is half the control (IC_{50}), (ii) the fraction of viable cells at the highest drug concentration (E_{max}), and (iii) the area under the dose–response curve (AUC)[6,7]. Dose–response and genomic datasets are often combined to discover drug-response biomarkers[1–3,8,9], but it has recently been found that large-scale drug-response data vary from one study to the next[10] for reasons that remain poorly understood[11–13].

We show here that, for dividing cells, traditional drug-response metrics such as IC_{50} suffer from a fundamental flaw when they are estimated from cell counts made at the end of the experiment (the standard approach): if control cells undergo different numbers of divisions during the course of an assay because of natural differences in proliferation rate, variation in growth conditions, or changes in the duration of an experiment, IC_{50}, E_{max}, and AUC values will vary dramatically, independently of any changes in the underlying biology. Thus, biomarkers that predict sensitivity under one (potentially arbitrary) set of assay conditions may not predict sensitivity under slightly different conditions. We therefore propose a new method for parameterizing drug response, the normalized growth rate inhibition (GR), which is based on the comparison of growth rates in the presence and absence of drug. Parameterization of GR data yields GR_{50}, GR_{max}, GR_{AOC}, and h_{GR} (Hill slope), values that are largely independent of cell division rate and assay duration (we use 'area over the curve', GR_{AOC}, rather than AUC for reasons discussed in Online Methods). GR metrics can be determined with modest changes in experimental procedures, and we propose that these metrics replace IC_{50} and E_{max} values in assessing cellular response to drugs, RNAi, and other perturbations in which control cells divide over the course of the assay.

RESULTS

Definition of normalized growth rate inhibition (GR)

We used computer simulation to model the drug response of three idealized cell lines with identical sensitivity to a cytostatic drug (i.e., a drug that arrests but does not kill cells) and different division times (T_d = 1.8, 2.4, or 3.9 d). These division times correspond to the lower quartile, median, and upper quartile for breast cancer cell lines[3] and are similar to the division times of NCI-60 cells[14]. In the slowly dividing cell line (T_d = 3.9 d), the total number of cells did not double in an assay typically run over 3 days, and thus E_{max} was ≥0.5, and IC_{50} was undefined. In the case of the two faster-growing cell lines, IC_{50} and E_{max} values fell as division rate increased (**Fig. 1a**) because cell number (or CTG value) was normalized to a drug-naïve control in which cell number increased as division time fell (compare curves across panels of **Fig. 1a**).

We can compensate for the confounding effects of division rate on drug-response measurements by computing the GR value at time t in the presence of drug at concentration c:

$$GR(c,t) = 2^{k(c,t)/k(0)} - 1$$

[1]HMS LINCS Center Laboratory of Systems Pharmacology, Department of Systems Biology, Harvard Medical School, Boston, Massachusetts, USA. [2]These authors contributed equally to this work. Correspondence should be addressed to P.K.S. (peter_sorger@hms.harvard.edu).

RECEIVED 2 OCTOBER 2015; ACCEPTED 1 APRIL 2016; PUBLISHED ONLINE 2 MAY 2016; DOI:10.1038/NMETH.3853

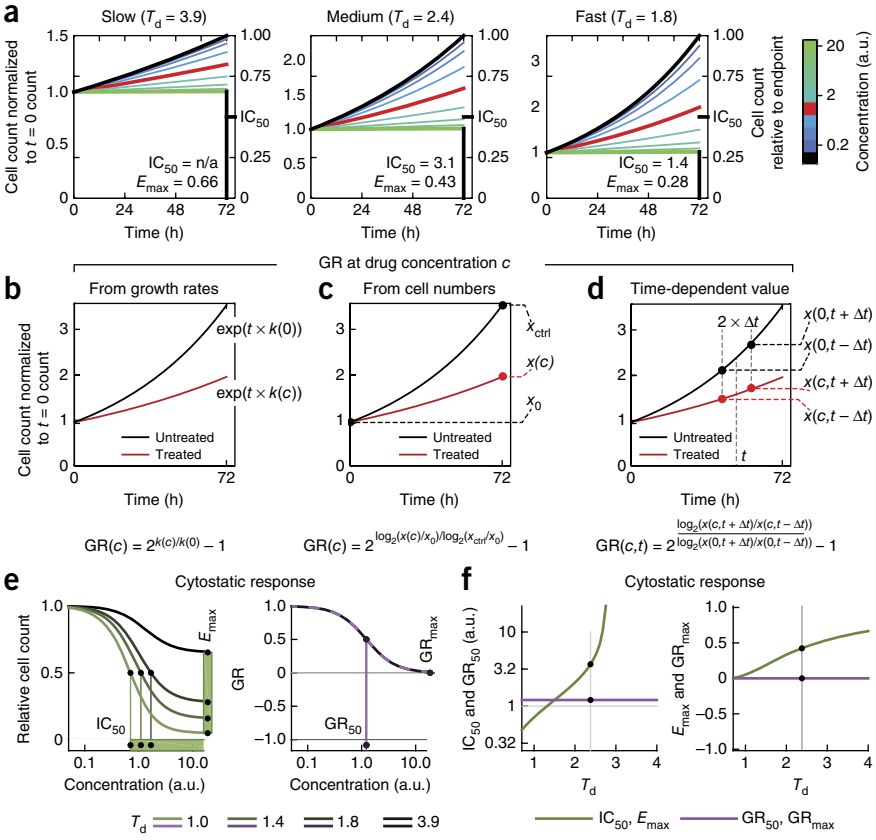

Figure 1 | Modeling drug response and the dependence of drug-response metrics on division time (T_d, values given in days). (**a**) Simulation of a simple drug-response model yields relative cell counts across a concentration range for a cytostatic drug for a slow- (left), medium- (middle), and fast-growing cell line (right). Black lines correspond to untreated control samples and red lines denote 50% growth inhibition. Black marks show where IC_{50} and E_{max} are evaluated. n/a, not applicable. a.u., arbitrary units. (**b**–**d**) Methods for evaluating GR value: (**b**) conceptual approach based on growth rates (k_0 and $k(c)$), (**c**) fixed-interval approach based either on cell number at the start (x_0) and end of the experiment (x_{ctrl} and $x(c)$) and (**d**) time-dependent value based on cell count before and after a time interval $2 \times \Delta t$ ($x(c,t \pm \Delta t)$). (**e**) Simulated data showing relative cell count (green lines) and GR value (purple lines) for a cytostatic drug assayed over 3 d. The darker the line, the longer the division time (given in days; see key below); note that all GR curves overlap. IC_{50} and GR_{50} are projected onto the x-axis; E_{max} and GR_{max} are projected onto the y-axis. (**f**) IC_{50} or E_{max} (green) and GR_{50} or GR_{max} (purple) computed from a theoretical 3-day assay for cells with division time ranging from 1 to 4 d; vertical line shows T_d = 2.4 d (AUC and GR_{AOC} values in **Supplementary Fig. 1c**).

where $k(c,t)$ is the growth rate of drug-treated cells and $k(0)$ is the growth rate of untreated control cells (**Fig. 1b**). The GR value is simply the ratio between growth rates under treated and untreated conditions normalized to a single cell division. The sign of the GR value relates directly to response phenotype: it lies between 0 and 1 in the case of partial growth inhibition, it equals 0 in the case of complete cytostasis, and it lies between 0 and −1 in the case of cell death. Given GR values for a range of drug concentrations, GR_{50} is the concentration at which $GR(c) = 0.5$, GR_{max} is the maximal measured GR value, and h_{GR} is the slope of the sigmoidal fit; GR_{AOC} is calculated by integrating the GR curve over a range of concentrations (Online Methods).

In practice, GR values can be estimated from endpoint measurement of cell number in treated and untreated samples, given the initial cell number (**Fig. 1c**; this is related to the procedure for GI_{50} determination, see **Supplementary Note**). Alternatively, the doubling time for untreated cells can be measured under the same conditions in parallel experiments and used in place of the initial cell number (Online Methods). A time-dependent GR value can be evaluated given cell count measurements at two or more time points. Time-dependent GR values capture adaptive responses, varying kinetics of drug–target interaction, drug efflux, etc. (**Fig. 1d**). Introducing time as a variable makes it possible to relate drug-induced changes in cell states to dynamic measures of drug response at a molecular level (equations for all calculations are provided in Online Methods with links to scripts).

To compare GR dose–response curves to conventional curves, we created synthetic data for cells that had T_d ranging from 1 to 4 d and that were exposed to a drug that was partially cytostatic, fully cytostasic, or cytotoxic (models are described in Online Methods). For all three drugs, IC_{50} and E_{max} values were strongly correlated with division time and assay duration, but this was not true of corresponding GR metrics (**Fig. 1e**,**f**; **Supplementary Fig. 1a**,**b**; and Online Methods). In the case of drugs that kill cells rapidly and independently of cell cycle state, GR_{max} still varies with growth rate, and time-dependent GR values are preferable (**Supplementary Fig. 2** and Online Methods). AUC combines IC_{50} or E_{max} data and is less sensitive to experimental noise[1,6,11], but it suffers from the same dependence on cell division time; GR_{AOC} corrects for this (**Supplementary Fig. 1c**).

GR metrics are robust to experimental variability

To study how changing cell division affects IC_{50} values, we expressed $BRAF^{V600E}$ in hTERT-immortalized retinal pigment epithelial (RPE) cells and then exposed them to etoposide, a topoisomerase II inhibitor that has a cytostatic effect in RPE cells (and whose mechanism of action is independent of BRAF). Oncogene overexpression is known to slow the growth of non-transformed cells[15,16], and expression of $BRAF^{V600E}$ in RPE cells under the control of a doxycycline-inducible promoter was observed to increase division time three-fold as the doxycycline concentration increased from 0 to 60 nM. Under these conditions the estimated IC_{50} value for etoposide increased 100-fold and E_{max} increased from 0.25 to 0.6 (**Fig. 2a** and **Supplementary Fig. 3a**). In contrast, GR_{50} and GR_{max} values varied only slightly under these conditions because the effects of etoposide per cell division were unchanged.

In a second experiment, we measured etoposide sensitivity in MCF 10A cells grown in serum-free medium supplemented with different concentrations of epidermal growth factor (EGF).

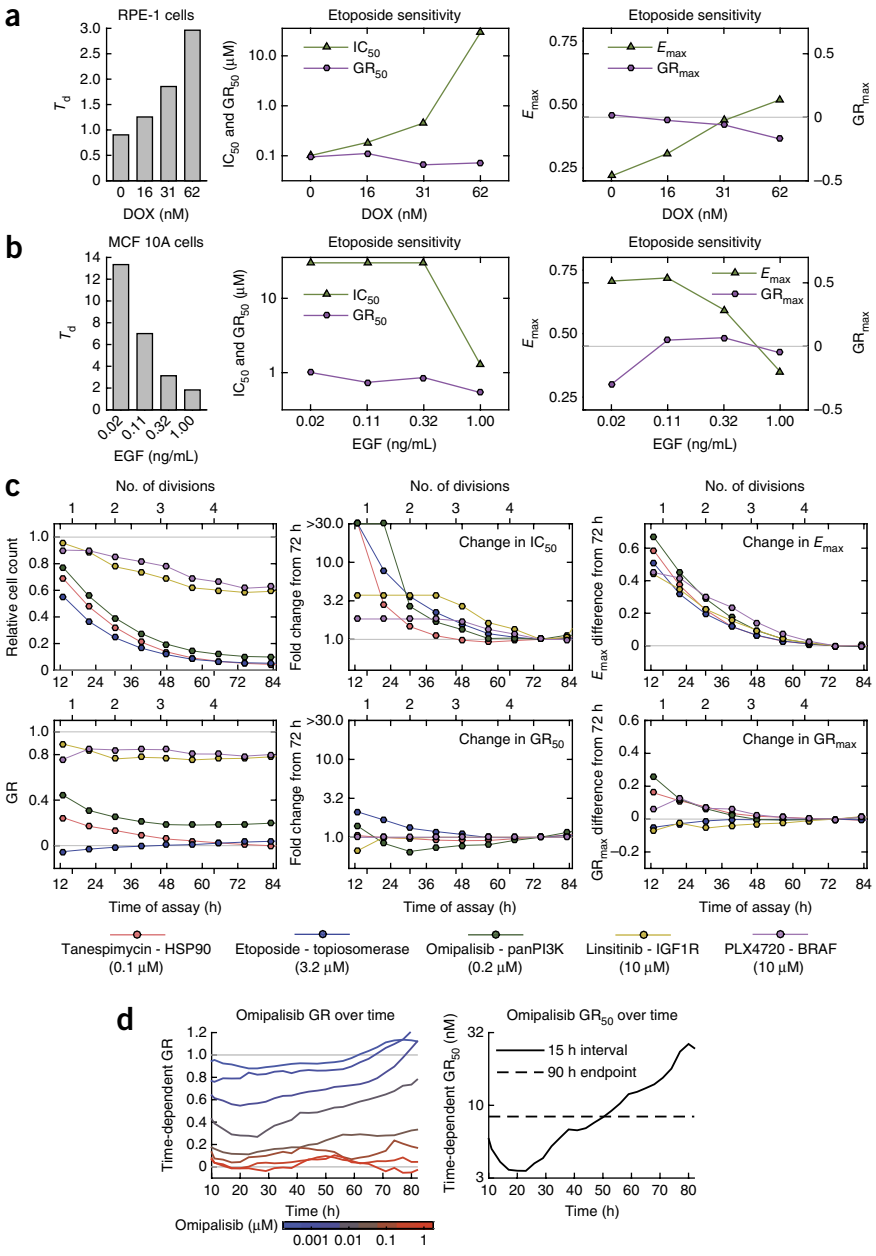

Figure 2 | GR values are independent of both the length of the assay and the division time. (**a**) Effect of altering T_d of hTERT RPE-1 cells on metrics of etoposide sensitivity. Relationship between T_d and doxycycline (DOX) concentration (left) to cells expressing $BRAF^{V600E}$ under the control of a DOX-regulated promoter. Values for IC_{50} and GR_{50} (middle) and E_{max} and GR_{max} (right) were evaluated at 48 h at different concentrations of DOX. Large and undefined values for IC_{50} were set at 30 μM for purposes of illustration. (**b**) Effect of altering T_d of MCF 10A cells on metrics of etoposide sensitivity. Relationship between T_d and concentration of EGF in serum-free medium (left). Values for IC_{50} and GR_{50} (middle) and E_{max} and GR_{max} (right) were evaluated at 59 h at different concentrations of EGF in serum-free medium. Large and undefined values for IC_{50} were set at 30 μM for purposes of illustration. (**c**) Evaluation of relative cell count (top) and GR values (bottom) for a drug concentration close to the GR_{50} value (left) and computed response metrics at different time points (middle and right), as estimated from live-cell imaging of MCF 10A cells exposed to one of five drugs with different mechanisms of action. (**d**) Time-dependent GR values estimated over 18-h intervals for MCF 10A cells grown as spheroids treated with omipalisib (left) and corresponding time-dependent GR_{50} values (right). Dashed line shows the GR_{50} value evaluated at 90 h. In all panels, the data shown derive from one of three biological replicates.

The division time of MCF 10A cells varied from >10 d at 0.02 ng ml^{-1} EGF to <2 d at 1 ng ml^{-1} EGF (**Fig. 2c**). Across this range, IC_{50} and E_{max} for etoposide were substantially more variable than GR_{50} or GR_{max} values (**Fig. 2b** and **Supplementary Fig. 3b**). Thus, potentially arbitrary and unintended differences in cell culture conditions can lead to large variation in IC_{50} and E_{max} values that is unlikely to have a biological basis.

To test the GR approach in a typical small-scale drug sensitivity screen, we exposed MCF 10A and BT-20 cells (expressing H2B-mCherry to facilitate automated cell counting) to five different drugs chosen for diverse mechanisms of action. We measured cell number approximately every 8 h over 3 d using an automated microscope. Estimated IC_{50} and E_{max} values converged only after three divisions (~60 h), whereas GR metrics stabilized by the first division (<20 h for MCF 10A and ~36 h for BT-20; **Fig. 2c** and **Supplementary Fig. 3c**). This confirms that GR metrics are substantially less dependent on assay duration than are IC_{50} and E_{max}. In the case of very slow and uneven growth (by primary human tumor cells, for example), the stabilization of GR values within one cell division is likely to be a real advantage in obtaining reliable estimates of drug sensitivity.

When grown in 3D culture, MCF 10A cells are known to adapt to inhibitors of PI3K and mTOR (such as omipalisib), becoming less sensitive over time[17]. Endpoint measures of drug sensitivity do not report on such adaptive responses. However, when we monitored spheroids by live-cell imaging, we observed that the time-dependent GR and GR_{50} values were lowest ~20 h after omipalisib addition, and they increased ~10-fold by day 4 (**Fig. 2d**); endpoint GR_{50} values lay midway in this range (**Fig. 2d**). Thus, time-dependent GR data directly capture the decreasing effectiveness of omipalisib in MCF 10A spheroids, enabling detection and further analysis of adaptive mechanisms.

Analysis of high-throughput data using GR metrics

The majority of large-scale drug-response datasets published to date neither report cell division rates nor allow one to estimate them. An exception is a study by Heiser *et al.*[3], which recorded cell numbers for breast cancer cell lines before and after exposure to a panel of anticancer drugs for 3 days. For many drugs in this dataset, IC_{50} correlates with division rate[6] (e.g., for cell cycle inhibitors, regression coefficient of −0.54, Spearman's P-value < 10^{-66}, N = 2,956;

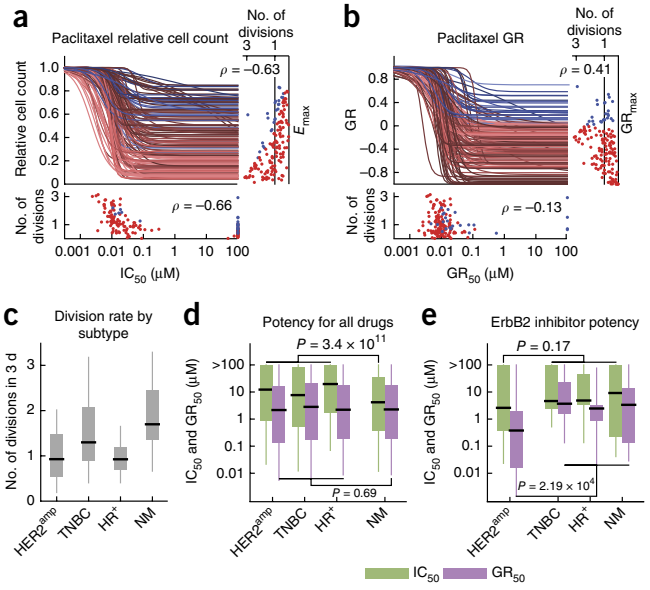

Figure 3 | Evaluation of GR metrics in a high-throughput dataset. (**a**,**b**) Fitted dose–response curves for (**a**) relative cell count and (**b**) GR values for paclitaxel in breast cancer cell lines (3-day assay data from Heiser *et al.*[3]). Red denotes cytotoxic response and blue denotes cytostatic response; darker curves denote cell lines with fewer divisions. Marginal distributions (below and to the right of the dose–response plots) show the relation between estimated IC_{50} or GR_{50} and E_{max} or GR_{max} values and number of divisions for that line over 3 d; ρ-values are Spearman's correlation coefficients. (**c**) Number of divisions over 3 d for cell lines in the dataset grouped by subtype: HER2-amplified ($HER2^{amp}$), triple-negative breast cancer (TNBC), hormone receptor positive (HR^+), and nonmalignant (NM). (**d**,**e**) Distribution of IC_{50} (green) and GR_{50} (purple) for all drugs in Heiser *et al.*[3] (**d**) or for ErbB2 inhibitors only (**e**) grouped by clinical subtype. *P*-values were derived from a rank-sum test for IC_{50} or GR_{50} values for NM cell (**d**) or for $HER2^{amp}$ cell lines (**e**) versus all other subtypes.

Supplementary Fig. 4a). However, we could reproduce this correlation by using an idealized model that does not assume any biological connection between drug sensitivity and division rate and by repeatedly simulating drug responses using random parameters (**Supplementary Fig. 4b** and Online Methods). This finding suggests that the correlation between drug sensitivity and division rate found in experimental data is spurious; also, the correlation was absent when drug response was measured using GR_{50} (Spearman's *P*-value = 0.31, **Supplementary Data 1**), suggesting that it is an artifact of the way IC_{50} is calculated.

Paclitaxel, a taxane microtubule inhibitor widely used in chemotherapy, is one drug that exhibits a strong negative correlation between sensitivity and division rate as well as substantial variation (100-fold) in IC_{50} across cell lines (**Fig. 3a**). This relationship has previously been described and is thought to arise because paclitaxel acts primarily on mitotic cells, and the faster a cell line divides, the more likely it is to be in mitosis[18,19]. However, reanalysis of data in Heiser *et al.*[3] shows that GR_{50} values for paclitaxel actually span a narrow range centered around 10 nM (**Fig. 3b** and **Supplementary Fig. 4c**), close to the estimated affinity of paclitaxel for assembled microtubules *in vitro*[20]. In contrast, GR_{max} values for paclitaxel vary considerably across cell lines and subtypes. In HER2-amplified ($HER2^{amp}$) and triple-negative breast cancer (TNBC) lines GR_{max} values are negative, which is indicative of a cytotoxic response, whereas hormone receptor-positive (HR^+) and nonmalignant lines generally exhibit cytostatic responses (**Supplementary Fig. 4c**). This is consistent with data showing that $HER2^{amp}$ and TNBC (basal-like) human tumors are more taxane-sensitive than tumors in other types of breast cancer[21]. We propose that future attempts to find biomarkers predictive of paclitaxel response focus on variation in GR_{max} rather than variation in IC_{50}[22,23].

The average division rate of breast cancer cell lines in culture differs with clinical subtype: among cells studied by Heiser *et al.*[3], HR^+ and $HER2^{amp}$ subtypes divided most slowly (median $T_d = 3.2$ d), TNBC cells divided faster (median $T_d = 2.3$ d), and nonmalignant cells divided still faster (median $T_d = 1.8$ d, **Fig. 3c**). As measured by IC_{50} values, nonmalignant cells were, on average, more sensitive to anticancer drugs than tumor cells, whereas GR_{50} values showed that the mean and range of drug sensitivity was similar (**Fig. 3d**). Focusing on $HER2^{amp}$ lines, IC_{50} values for inhibitors of EGFR and ErbB2 were similar across breast cancer subtypes, even though $HER2^{amp}$ human tumors are preferentially sensitive to such drugs and ErbB2 inhibitors are frontline therapy for this disease[24,25]. GR_{50} data for $HER2^{amp}$ cell lines in Heiser *et al.* show that this subtype of breast cancer is ~10-fold more sensitive than other subtypes to EGFR/ErbB2 inhibitors *in vitro* (**Fig. 3e**; $P = 1.3 \times 10^{-4}$). The failure of IC_{50} values to show the preferential sensitivity of $HER2^{amp}$ cell lines to EGFR/ErbB2 inhibitors arises because their relatively slow growth rate is a hidden confounder in IC_{50} calculation. From these data we conclude that artefactual dependency of IC_{50} on cell division rate creates associations where none exist and also obscures meaningful associations between genotype and drug sensitivity.

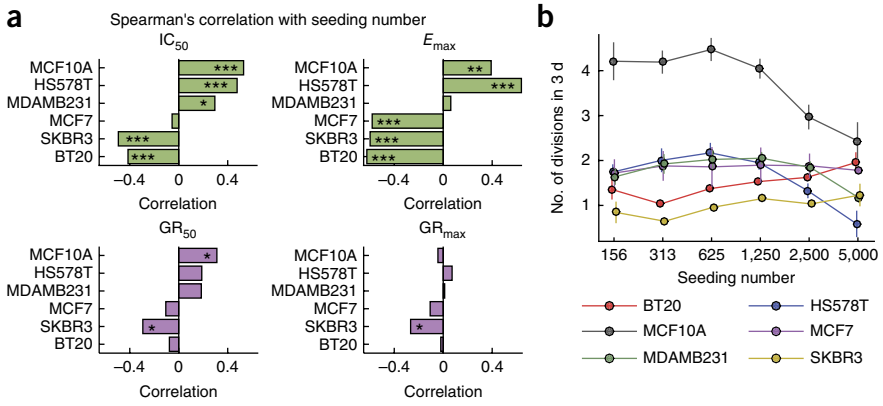

Figure 4 | Plating density affects division rate and drug sensitivity. (**a**) Spearman's correlation between estimated values for IC_{50}, E_{max}, GR_{50}, and GR_{max} and seeding number for the six breast cancer cell lines shown. Data derive from an experiment in which cells were plated at a range of six densities and treated with 11 drugs having diverse mechanisms of action (Online Methods and **Supplementary Data 2**). Significance: $^*P < 0.05$, $^{**}P < 0.01$, $^{***}P < 0.001$. (**b**) Relationship between seeding number and the number of divisions in 3 d. Error bars are the s.e.m. of five to nine biological replicates.

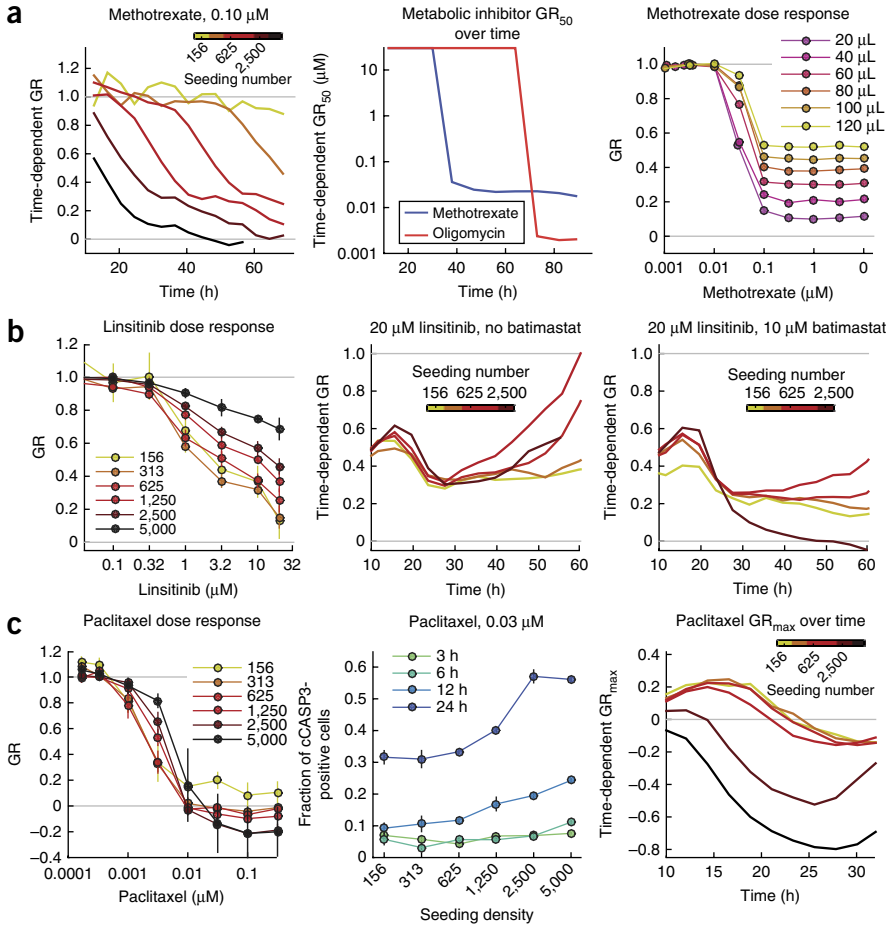

Figure 5 | Time-dependent GR metrics reveal diverse mechanisms of drug sensitivity and resistance. Evaluation of three selected drugs for which seeding density had a significant effect on GR values in MCF 10A cells based on data summarized in **Figure 4**. (**a**) Influence of ratio of cell number to medium volume for two drugs related to metabolism. Time-dependent GR values for MCF 10A cells at different seeding numbers following exposure to 0.1 μM methotrexate (left). Time-dependent GR_{50} values for MCF 10A cells for methotrexate or oligomycin (middle); values are capped at 30 μM for illustration purposes. GR dose–response curves at 3 d for MCF 10A treated with methotrexate with a constant number of seeded cells but in different volumes of medium (right). Data shown derive from one of two biological replicates. (**b**) Medium conditioning and adaptive resistance to linsitinib, an IGF1R inhibitor. GR dose–response curves at 3 d for MCF 10A treated with linsitinib at different cell densities (left). Error bars are the s.e.m. of three biological replicates. Time-dependent GR values for MCF 10A at different seeding numbers following exposure to 20 μM linsitinib in the absence (middle) or presence (right) of 10 μM batimastat, a matrix metalloproteinase inhibitor. Data shown are from one of three biological replicates. (**c**) Paclitaxel-induced cytostasis at low cell density and apoptosis at high cell density. GR values for MCF 10A cells seeded at different densities and treated with paclitaxel for 3 d (left). Error bars are the s.e.m. of three biological replicates. Fraction of MCF 10A cells positive for cleaved caspase-3 at different time points and cell densities following exposure to 0.03 μM paclitaxel (middle). Time-dependent GR_{max} values for paclitaxel in MCF 10A cells seeded at different densities (right). Data shown are from one of two biological replicates.

Effects of cell density on drug sensitivity

GR metrics allow us to quantify how drug sensitivity changes in the face of variables that affect division rate. One such variable is seeding density: increasing density has widely been reported to promote drug resistance[26–29]. To investigate this, we cultured six breast cell lines representative of different subtypes at six seeding densities over a 32-fold range. 24 h after plating, cells were exposed to 11 drugs with diverse mechanisms of action. Growth rates, IC_{50}, E_{max}, and GR metrics were estimated by imaging and counting fixed cells at the time of drug addition and 72 h after treatment (**Supplementary Data 2**). Overall, IC_{50} and E_{max} correlated positively with seeding number for MCF 10A, MDA-MB-231, and Hs 578T cells, and they correlated negatively for BT-20 and SK-BR-3 cells ($P < 0.01$, **Fig. 4a**). In the first three cell lines, division rate decreased with density, presumably because of contact inhibition, depletion of essential medium components, and other effects (**Fig. 4b**)[30–32]. In BT-20 and SK-BR-3 cells, division rate increased with density, presumably because of conditioning of the growth medium[31,33]. Correlations between density and IC_{50} and E_{max} were weakest for MCF7 cells, which grew equally well across all densities. Thus, the effect of density on number of divisions, and consequently on IC_{50} and E_{max}, varied dramatically among cell lines (**Supplementary Fig. 5a**). However, only a small number of cell line–drug pairs exhibited a statistically significant association between plating density and GR_{50} or GR_{max} values. We wondered whether these were situations in which the biology of drug response was altered by density.

In MCF 10A cells, six drugs were associated with significant variation in GR_{50} or GR_{max} (or both) across seeding densities; RNA-seq revealed that gene expression in these cells also varied with cell density, with significant enrichment for genes involved in catabolic processes, cellular respiration, and wounding responses[30–32,34] (**Supplementary Fig. 6a**). When the data was analyzed by principal-component analysis, the first principal component (which captured 32% of variance) was strongly correlated with the number of cells at the time of collection (Spearman's $\rho = 0.98$) and less so with time in culture ($\rho = 0.57$), suggesting that the cell density at the time of assay and not the history of the culture was the primary determinant of transcriptional state (**Supplementary Fig. 6b**). Follow-up studies with methotrexate showed that the ratio between cell number and medium volume, and not cell density per se, was the key variable for sensitivity to this drug (this was also true of oligomycin, an inhibitor of ATP synthase; **Fig. 5a** and **Supplementary Fig. 7**); since cells grew in a constant volume of medium, GR_{50} was therefore time dependent. Density- (and time-) dependent variation in GR_{50} were also observed for linsitinib, an IGF1R inhibitor currently in Phase II clinical trials (**Fig. 5b**). Variation in GR_{50} with time and density was reduced by cotreatment with the metalloprotease inhibitor

batimastat, suggesting a role for autocrine conditioning of the microenvironment in drug response.

In the case of paclitaxel, GR_{50} values remained at ~5–10 nM across plating densities, but GR_{max} was strongly density dependent, varying from ~0 (cytostatic) at low cell densities to negative values (cytotoxic) at higher densities (**Fig. 5c**, left). Time-dependent GR_{max} reached its greatest negative value at 24 h, concomitant with an increase in the fraction of taxol-treated cells that contain cleaved caspase-3, confirming that negative GR_{max} values corresponded to elevated apoptosis (**Fig. 5c**, middle and right). Though its molecular basis is unknown, this effect may be one reason for the discrepancy between cell-killing dynamics in low-density culture and in high-density xenograft tumors[35].

DISCUSSION

Accurate measurement of drug sensitivity and resistance is the cornerstone of cancer biology, pharmacology, and of many fundamental studies on cell signaling and cell division. In this paper we demonstrate theoretically and experimentally that variation in division rate seriously confounds existing drug-response metrics. We also show that division rate varies with cell type, medium composition, and seeding density, often in unpredictable ways. Cell division rate slows down in some cell lines as density increases, while it speeds up in others. Such variation can change apparent IC_{50} 100-fold or more and therefore introduce artificial correlations in data, obscure the true effects of drug action, and introduce unknown complications into biomarker discovery. As an alternative, we propose GR metrics that are computed by comparing growth rates in the presence and absence of drug. GR_{50} and GR_{max} are robust to variation in cell division rate and should replace IC_{50} and E_{max} in studies in which control cells divide (including the study of drugs, gene depletion or overexpression, and variation in the extracellular environment). GR_{50} quantifies the potency of a drug on a per-division basis, ensuring that fast- and slow-growing cells with similar biochemical responses to drug are scored equivalently. GR_{max} captures the maximal drug effect on growth rate and differs from E_{max} in that it falls between 1 and −1, where negative values denote cell death, 0 denotes cytostasis, and positive values denote partial inhibition. GR_{AOC} and h_{GR} values can also be calculated from GR curves; the former is often the most robust metric in the face of experimental noise, and the latter quantifies an important relationship between dose and response that is often neglected[6].

In the simplest version of our method, GR metrics are computed after measuring cell number or a surrogate (e.g., CTG value) before and after exposure of a culture to varying concentrations of drug or other perturbation for a fixed time (**Fig. 1c**). When cell division rates under similar culture conditions are known from previous data, only the final cell number is needed (although we believe that before and after data on cell number are a valuable control to ensure data quality). Time-course data make it possible to compute time-dependent GR values and to quantify phenomena such as delayed response, drug adaptation, or variation in the kinetics of drug–target interaction (**Fig. 1d**). To facilitate the use of GR metrics by others we provide MATLAB and python routines and an online GR calculator (http://www.grcalculator.org/). Moreover, the data in this paper, including the GR_{50} and GR_{max} values for the Heiser *et al.* dataset, are available online (http://lincs.hms.harvard.edu/).

Large-scale drug-response studies based on existing response metrics[1,2,8,9] are discrepant for poorly understood reasons[5,11,12], raising concerns about the value of drug-response biomarkers[10]. We speculate that comparison of datasets across centers (or even within a center) might be confounded by differences in plating density, growth medium, and other factors that affect cell division rate. It might be possible to correct for this in existing data by computing GR values post facto, but this will require recreating the original assay conditions and then measuring division rates.

Based on the results in this paper, we believe that use of GR metrics in lieu of traditional IC_{50}, E_{max}, or AUC values will improve our ability to identify genes and biological processes responsible for drug sensitivity and resistance. GR metrics decouple any effect that genotype or microenvironment have on division rate from their effect on drug sensitivity. Cell biology studies involving the modification of genes or the microenvironment often result in changes in cell division rate, leading to potentially spurious correlations with drug sensitivity (as illustrated here by oncogene overexpression and changes in EGF levels), and should also benefit from the use of GR metrics. By analogy with antimicrobial susceptibility testing for bacterial infections, it has recently been suggested that cancer therapy might be personalized by screening primary human tumor cells against panels of drugs[36,37]. Such cells grow slowly and unevenly in culture, making division number a poorly controlled variable. Accounting for such differences using GR metrics should create drug-response data that are more reproducible and useful for optimizing patient therapy.

METHODS

Methods and any associated references are available in the online version of the paper.

Accession codes. Data are deposited in the Gene Expression Omnibus (GEO) database with accession number GSE80297.

Note: Any Supplementary Information and Source Data files are available in the online version of the paper.

ACKNOWLEDGMENTS

This work was funded by grants U54-HL127365 and P50-GM107618 to P.K.S. and by a fellowship from the Swiss National Science Foundation (P300P3_147876) to M.H. We thank M. Soumillon for expression profiling, J. Chen (Department of Systems Biology, Harvard Medical School, Boston, Massachusetts, USA) for the modified RPE-1 cells and A. Palmer, M. Eisenstein, and G. Berriz for help with the manuscript.

AUTHOR CONTRIBUTIONS

M.H., M.N., and P.K.S. conceived this study and wrote the paper. M.N., M.C., and M.H. performed the experiments; M.H. conceived GR metrics and performed the computational analyses.

COMPETING FINANCIAL INTERESTS

The authors declare no competing financial interests.

1. Barretina, J. *et al.* The Cancer Cell Line Encyclopedia enables predictive modelling of anticancer drug sensitivity. *Nature* **483**, 603–607 (2012).
2. Garnett, M.J. *et al.* Systematic identification of genomic markers of drug sensitivity in cancer cells. *Nature* **483**, 570–575 (2012).
3. Heiser, L.M. *et al.* Subtype and pathway specific responses to anticancer compounds in breast cancer. *Proc. Natl. Acad. Sci. USA* **109**, 2724–2729 (2012).

4. Schenone, M., Dančík, V., Wagner, B.K. & Clemons, P.A. Target identification and mechanism of action in chemical biology and drug discovery. *Nat. Chem. Biol.* **9**, 232–240 (2013).
5. Cravatt, B.F. & Gottesfeld, J.M. Chemical biology meets biological chemistry minireview series. *J. Biol. Chem.* **285**, 11031–11032 (2010).
6. Fallahi-Sichani, M., Honarnejad, S., Heiser, L.M., Gray, J.W. & Sorger, P.K. Metrics other than potency reveal systematic variation in responses to cancer drugs. *Nat. Chem. Biol.* **9**, 708–714 (2013).
7. Sebaugh, J.L. Guidelines for accurate EC50/IC50 estimation. *Pharm. Stat.* **10**, 128–134 (2011).
8. Rees, M.G. *et al.* Correlating chemical sensitivity and basal gene expression reveals mechanism of action. *Nat. Chem. Biol.* **12**, 109–116 (2016).
9. Seashore-Ludlow, B. *et al.* Harnessing connectivity in a large-scale small-molecule sensitivity dataset. *Cancer Discov.* **5**, 1210–1223 (2015).
10. Errington, T.M. *et al.* An open investigation of the reproducibility of cancer biology research. *eLife* **3**, e04333 (2014).
11. Haibe-Kains, B. *et al.* Inconsistency in large pharmacogenomic studies. *Nature* **504**, 389–393 (2013).
12. Safikhani, Z. *et al.* Revisiting inconsistency in large pharmacogenomic studies. Preprint at http://dx.doi.org/10.1101/026153 (2015).
13. The Cancer Cell Line Encyclopedia Consortium & the Genomics of Drug Sensitivity in Cancer Consortium. Pharmacogenomic agreement between two cancer cell line data sets. *Nature* **528**, 84–87 (2015).
14. O'Connor, P.M. *et al.* Characterization of the p53 tumor suppressor pathway in cell lines of the National Cancer Institute anticancer drug screen and correlations with the growth-inhibitory potency of 123 anticancer agents. *Cancer Res.* **57**, 4285–4300 (1997).
15. Serrano, M., Lin, A.W., McCurrach, M.E., Beach, D. & Lowe, S.W. Oncogenic ras provokes premature cell senescence associated with accumulation of p53 and p16INK4a. *Cell* **88**, 593–602 (1997).
16. Michaloglou, C. *et al.* BRAFE600-associated senescence-like cell cycle arrest of human naevi. *Nature* **436**, 720–724 (2005).
17. Muranen, T. *et al.* Inhibition of PI3K/mTOR leads to adaptive resistance in matrix-attached cancer cells. *Cancer Cell* **21**, 227–239 (2012).
18. Chabner, B.A., Allegra, C.J., Curt, G.A. & Calabresi, P. in *The Pharmacological Basis of Therapeutics* 9th edn. (eds. Hardman, J. & Limbird, L.) Ch. 51 (McGraw-Hill, 1996).
19. Baguley, B.C. *et al.* Resistance mechanisms determining the in vitro sensitivity to paclitaxel of tumour cells cultured from patients with ovarian cancer. *Eur. J. Cancer* **31A**, 230–237 (1995).
20. Caplow, M., Shanks, J. & Ruhlen, R. How taxol modulates microtubule disassembly. *J. Biol. Chem.* **269**, 23399–23402 (1994).
21. Rouzier, R. *et al.* Breast cancer molecular subtypes respond differently to preoperative chemotherapy. *Clin. Cancer Res.* **11**, 5678–5685 (2005).
22. Shi, J., Orth, J.D. & Mitchison, T. Cell type variation in responses to antimitotic drugs that target microtubules and kinesin-5. *Cancer Res.* **68**, 3269–3276 (2008).
23. Gascoigne, K.E. & Taylor, S.S. Cancer cells display profound intra- and interline variation following prolonged exposure to antimitotic drugs. *Cancer Cell* **14**, 111–122 (2008).
24. Konecny, G.E. *et al.* Activity of the dual kinase inhibitor lapatinib (GW572016) against HER-2-overexpressing and trastuzumab-treated breast cancer cells. *Cancer Res.* **66**, 1630–1639 (2006).
25. Moasser, M.M., Basso, A., Averbuch, S.D. & Rosen, N. The tyrosine kinase inhibitor ZD1839 ("Iressa") inhibits HER2-driven signaling and suppresses the growth of HER2-overexpressing tumor cells. *Cancer Res.* **61**, 7184–7188 (2001).
26. Chauffert, B. *et al.* New insights into the kinetic resistance to anticancer agents. *Cytotechnology* **27**, 225–235 (1998).
27. Dimanche-Boitrel, M.T., Garrido, C. & Chauffert, B. Kinetic resistance to anticancer agents. *Cytotechnology* **12**, 347–356 (1993).
28. Garrido, C. *et al.* Circumvention of confluence-dependent resistance in a human multi-drug-resistant colon-cancer cell line. *Int. J. Cancer* **61**, 873–879 (1995).
29. Fang, Y., Sullivan, R. & Graham, C.H. Confluence-dependent resistance to doxorubicin in human MDA-MB-231 breast carcinoma cells requires hypoxia-inducible factor-1 activity. *Exp. Cell Res.* **313**, 867–877 (2007).
30. Sorby, M. & Ostman, A. Protein-tyrosine phosphatase-mediated decrease of epidermal growth factor and platelet-derived growth factor receptor tyrosine phosphorylation in high cell density cultures. *J. Biol. Chem.* **271**, 10963–10966 (1996).
31. Kim, J.H., Kushiro, K., Graham, N.A. & Asthagiri, A.R. Tunable interplay between epidermal growth factor and cell-cell contact governs the spatial dynamics of epithelial growth. *Proc. Natl. Acad. Sci. USA* **106**, 11149–11153 (2009).
32. Curto, M., Cole, B.K., Lallemand, D., Liu, C.H. & McClatchey, A.I. Contact-dependent inhibition of EGFR signaling by Nf2/Merlin. *J. Cell Biol.* **177**, 893–903 (2007).
33. Kaplan, P.L., Anderson, M. & Ozanne, B. Transforming growth factor(s) production enables cells to grow in the absence of serum: an autocrine system. *Proc. Natl. Acad. Sci. USA* **79**, 485–489 (1982).
34. Sero, J.E. *et al.* Cell shape and the microenvironment regulate nuclear translocation of NF-κB in breast epithelial and tumor cells. *Mol. Syst. Biol.* **11**, 790 (2015).
35. Orth, J.D. *et al.* Analysis of mitosis and antimitotic drug responses in tumors by in vivo microscopy and single-cell pharmacodynamics. *Cancer Res.* **71**, 4608–4616 (2011).
36. Yuan, H. *et al.* Use of reprogrammed cells to identify therapy for respiratory papillomatosis. *N. Engl. J. Med.* **367**, 1220–1227 (2012).
37. Crystal, A.S. *et al.* Patient-derived models of acquired resistance can identify effective drug combinations for cancer. *Science* **346**, 1480–1486 (2014).

ONLINE METHODS

Metrics of drug response. *Determining relative cell counts.* Cell counts in the presence of drug are normalized to DMSO-treated controls grown on the same plate under the same conditions. In the current study, relevant conditions include seeding density, the concentration of exogenous growth factors (e.g., EGF in the case of MCF 10A cells), and the concentration of a second drug such as doxycycline or batimastat. For each cell line, drug, and drug concentration, we define the relative cell count as $x(c)/x_{ctrl}$, where $x(c)$ is the count in the presence of drug at concentration c and x_{ctrl} is the 50%-trimmed mean of the count for control cells. Technical replicates are averaged to yield an average relative cell count. We typically collect data from three technical replicates (on three separate plates).

Calculating GR values using endpoint drug-response data. Normalized growth rate inhibition is calculated according to the formula:

$$GR(c) = 2^{\frac{\log_2(x(c)/x_0)}{\log_2(x_{ctrl}/x_0)}} - 1 \textbf{ (Fig. 1c)},$$

where $x(c)$ and x_{ctrl} are as described above, and x_0 is the 50%-trimmed mean of the cell count from a sample grown in parallel and measured just prior to drug exposure.

Alternatively, the untreated division time $T_d = \ln(2)/k(0)$ can be measured in independent experiments and used in place of the initial cell number ($x_0 = x_{ctrl} \times 2^{-T/T_d}$):

$$GR(c) = 2^{1+\frac{\log_2(x(c)/x_{ctrl})}{T/T_d}} - 1,$$

where T is the duration of the assay.

Calculating time-dependent GR values. GR values can be evaluated over a time interval ($2 \times \Delta t$) around any time point t based on the equation:

$$GR(c,t) = 2^{\frac{\log_2(x(c,t+\Delta t)/x(c,t-\Delta t))}{\log_2(x(0,t+\Delta t)/x(0,t-\Delta t))}} - 1 \textbf{ (Fig. 1d)}.$$

The time-dependent GR values in the current paper were computed with $2 \times \Delta t = 12$ h to 18 h, which corresponds to about half a cell division time.

Curve fitting and estimating drug-response metrics. GR data are fitted to a sigmoidal curve as follows (**Supplementary Fig. 8b**):

$$GR(c) = GR_{inf} + \frac{1 - GR_{inf}}{1 + (c/GEC_{50})^{h_{GR}}}$$

where the fitted parameters are:

- GR_{inf}: the effect of the drug at infinite concentration ($GR_{inf} \equiv GR(c \to \infty)$). GR_{inf} lies between −1 and 1; negative values correspond to cytotoxic responses (i.e., induction of cell death, **Supplementary Fig. 8a**), a value of 0 corresponds to a fully cytostatic response (**Supplementary Fig. 8b**), and a positive value corresponds to partial growth inhibition (**Supplementary Fig. 8c**).
- h_{GR}: the Hill coefficient of the fitted curve, which reflects how steep the dose–response curve is. In practice, we typically constrain h_{GR} to a value between 0.1 and 5.
- GEC_{50}: the concentration at half-maximal effect. To avoid artefacts in curve fitting we constrain GEC_{50} to be two orders of magnitude higher and lower than the experimentally tested concentration range (in practice, this is usually about 10^{-5} to 10^3 μM).

If the fit of the curve is not significantly better than that of a flat curve (i.e., $GR(c) \equiv GR_{inf}$) based on an F-test with cutoff of $P = 0.05$, the response is considered flat and the parameter GEC_{50} is set to 0 (**Supplementary Fig. 8d**).

Inferred drug-response metrics. The GR_{50} value is the concentration of drug at which $GR(c = GR_{50}) = 0.5$. If the value for GR_{inf} is above 0.5, the GR_{50} value is not defined and is therefore set to $+\infty$ (**Supplementary Fig. 8c**). By extension, other thresholds can be defined in a similar manner. For example, GR_{100} corresponds to the concentration at which a drug is fully cytostatic: $GR(c = GR_{100}) = 0$.

The GR_{max} is the maximum effect of the drug at the highest tested concentration, and it lies between −1 and 1; a value of 0 corresponds to a fully cytostatic response, and a negative value corresponds to a cytotoxic response. GR_{max} can be estimated from the fitted curve or obtained directly from experimental data; we often do the latter.

For time course data, all metrics are evaluated at each time point individually.

Area under the curve and over the curve (GR_{AOC}). Another common metric for quantifying dose–response data is the area under the response curve (AUC), which is based on integrating the dose–response curve over the range of tested concentrations. In the case of GR curves, which can have negative values, it is more intuitive to use the area over the curve:

$$GR_{AOC} = \int 1 - GR(c)\,dc \cong 1 - \sum_{c_i} GR(c_i),$$

where $GR(c_i)$ are measured GR values at discrete concentrations c_i. GR_{AOC} has the benefit that, in the case of no response, it has a value of 0. The GR_{AOC} can be normalized to the range of concentrations as, for example, $GR_{AOC}/\log_{10}(c_{max}/c_{min})$, where c_{max} and c_{min} are the highest and lowest tested concentrations. It is important to note that GR_{AOC} values (like conventional AUC) should only be used to compare responses evaluated across the same drug concentration range.

The GR_{AOC} value captures variation in potency and efficacy at the same time. The calculation of GR_{AOC} at discrete (experimentally determined) concentrations has the advantage that it does not require curve fitting and is therefore free of fitting artifacts. This is especially useful for assays where fewer than five concentrations are measured, and curve fitting is unreliable. GR_{AOC} values are also more robust to experimental noise than metrics derived from curve fitting; GR_{max} values are particularly sensitive to outlier values when directly obtained from data.

doi:10.1038/nmeth.3853

Drug concentration range. The drug concentrations used for fitting drug-response curves need to span a sufficiently wide range and have sufficiently intermediate values in order to obtain reliable estimates for GEC_{50}, h_{GR}, and GR_{inf}. Denser sampling provides more precise estimates, especially in the case of steep dose–response curves. Optimal design of dose–response curves has been discussed elsewhere[7]. In practice, we suggest using nine doses spanning four orders of magnitude from 1 nM to 10 μM. This range can be shifted to lower concentrations for more potent drugs or to higher concentrations for less potent drugs with the caveat that GR_{AOC} values for different drugs should be compared only if evaluated over the same concentration range. We suggest discarding any GR_{50} value that is more than an order of magnitude above the highest tested concentration because values extrapolated from the fitted curves are more subject to fitting artefacts than interpolated values. Similarly, GR_{inf} value is not properly constrained if the GR(c) dose–response curve does not reach a plateau at the highest measured concentration. In such cases, GR_{AOC} is the most reliable metric.

Computing GR metrics. Source code for computing GR metrics is provided (**Supplementary Software**). To facilitate the computation of GR metrics we provide updated source code available under an open source software license and MATLAB and python scripts at https://github.com/sorgerlab/gr50_tools. We also provide an online calculator at http://www.grcalculator.org. This website contains a user guide, various tutorials and explanatory materials, and example datasets, including all of the data in the current manuscript.

Theoretical model of drug response. To simulate the effect of division time on GR and conventional drug-response metrics under different assumptions about the degree of cytostasis or cell killing, we developed a theoretical model of drug response. To the first approximation, cell growth can be considered exponential, with drugs either decreasing the division rate or killing cells in a cell-cycle-dependent manner:

$$\dot{x} = x \times k\left(1 - \frac{S_M \times c^h}{SC_{50}^h + c^h}\right),$$

where x is the cell count, k is the untreated growth rate (per day), c is the drug concentration, S_M is the maximal inhibitory effect, SC_{50} is the concentration at half-maximal effect of drug, and h is the Hill coefficient. The growth rate k corresponds to the division rate k_0 as $k = \ln(2) \times k_0 = \ln(2)/T_d$, where T_d is the division time. S_M can be larger than 1 to account for drugs inducing cell death at a specific phase of the cell cycle. The model can also be generalized to account for drugs that induce cell death independent of the cell cycle:

$$\dot{x} = x \times k\left(1 - \frac{S_M \times c^h}{SC_{50}^h + c^h}\right) - x \times \left(\frac{k_L \times c^h}{LC_{50}^h + c^h}\right),$$

where k_L is the maximal killing rate (per day) and LC_{50} is the concentration of drug that produces half-maximal cell killing. Integrating these equations for an assay of t days yields the cell count at concentration c:

$$x(c,t) = x_0 \times \exp\left(t \times k\left(1 - \frac{S_M \times c^h}{SC_{50}^h + c^h}\right) - t\frac{k_L \times c^h}{LC_{50}^h + c^h}\right),$$

where $x_0 \equiv x(t = 0)$ is the cell number at the time of treatment. Thus, the relative cell count is:

$$IC(c,t) = x(c,t)/x_{ctrl} = \exp\left(-t \times k\frac{S_M \times c^h}{SC_{50}^h + c^h} - t\frac{k_L \times c^h}{LC_{50}^h + c^h}\right),$$

where $x_{ctrl} \equiv x(0,t)$,

and the normalized growth rate inhibition (GR value) is:

$$GR(c,t) = 2^{\left(\frac{\log_2 x(c,t)/x_0}{\log_2(x_{ctrl}/x_0)}\right)} - 1 = 2^{\left(1 - \frac{S_M \times c^h}{SC_{50}^h + c^h} - \frac{1}{k}\frac{k_L \times c^h}{LC_{50}^h + c^h}\right)} - 1.$$

This equation for GR(c) is independent of the length of the assay t and, thus, the metrics GR_{50}, GR_{max}, GR_{AUC} , and h_{GR} are also independent of t. For cases where drug action is mainly related to the cell cycle ($k_L = 0$), GR values are also independent of the untreated growth rate k. As shown in **Supplementary Figures 2** and **3a**,**b**, the impact of $k_L > 0$ is minimal on GR_{50} and relatively small on GR_{max}. This is also illustrated by the analytical formula for GR_{inf}: $GR_{inf} = 2^{(1 - S_M - k_L/k)} - 1$. Note that the metrics derived from growth inhibition (GI) values used in Heiser *et al.*[3], such as GI_{50}, are more robust than traditional metrics, but they still depend on both division time and assay length (see **Supplementary Note**).

Parameters for simulations in figure panels. Model parameters used in the numerical simulations shown in the main and supplemental figures (**Fig. 1b**; **Supplementary Figs. 1**, **2**, and **7**) were as follows:

- Cytostatic: $S_M = 1$, $S_{50} = 1.5$, $T_M = 0$, $h = 1.6$
- Partial response: $S_M = 0.65$, $S_{50} = 1.2$, $T_M = 0$, $h = 1.6$
- Cytotoxic: $S_M = 2.6$, $S_{50} = 2$, $T_M = 0$, $h = 1.6$
- Partial toxic response: $S_M = 0.45$, $S_{50} = 1.2$, $T_M = 0.05$, $T_{50} = 5$, $h = 1.6$
- Mixed response: $S_M = 0.65$, $S_{50} = 1.2$, $T_M = 0.1$, $T_{50} = 3$, $h = 1.6$
- Complete cytotoxic: $S_M = 2.6$, $S_{50} = 1.2$, $T_M = 1$, $T_{50} = 3$, $h = 1.6$

For **Supplementary Figure 3b**, the parameters were randomly sampled within the following distribution:

- Division rate k: normal distribution around 0.9 divisions per day with s.d. of 0.46 and a lower bound of 0.14
- Hill coefficient h: uniform distribution between 1.5 and 2.5
- Maximum inhibition S_M: uniform distribution between 0 and 2
- Half inhibition concentration S_{50}: log-uniform distribution ranging from 0.31 to 10

- Maximum toxic effect T_M: 0 for 50% of values, uniform distribution between 0 and 0.5 for the other 50% of values
- Half inhibition concentration T_{50}: log-uniform distribution ranging from 0.56 to 5.6

Experimental methods and data processing. *Cell lines and tissue culture.* MCF 10A, Hs 578T, MDA-MB-231, MCF7, SK-BR-3, and BT-20 were obtained from the ATCC and grown according to ATCC recommendations. For time-lapse experiments, MCF 10A and BT-20 cells were modified by inserting an H2B-mCherry expression cassette (gift of R. Benezra, Addgene plasmid # 20972)[38] that comprised AAVS1 homology arms, the hPGK promotor, and SV40 polyA terminator (gift from R. Jaenisch, Addgene plasmid # 22072)[39] into the AAVS1 safe harbor genomic locus using CRISPR/Cas9. MCF 10A-H2B-mCherry cells were grown in the same manner as the parental strain, with the exception that traditional DMEM was replaced with FluoroBrite DMEM (Thermo Fisher Scientific) for imaging. The modified hTERT RPE-1 cells (gift from J. Chen) were created by inserting the full-length $BRAF^{V600E}$ expression cassette (Addgene plasmid # 15269)[40] driven by a tet-inducible promotor (Addgene plasmid # 41394). Cell identity was confirmed by short tandem repeat (STR) profiling at the Dana-Farber Cancer Institute, and all cells were tested with the MycoAlert PLUS mycoplasma detection kit (Lonza) and found to be free of mycoplasma prior to analysis.

Drugs and dyes. Drugs were obtained from commercial vendors and tested for purity inhouse as described in detail in the HMS LINCS drug collection database (http://lincs.hms.harvard.edu/db/sm/). Drugs and reporter dyes were dispensed directly into multiwell plates using a D300 Digital Dispenser (Hewlett-Packard). To stain cells, YOYO-1 and TOTO-3 (Thermo Fisher Scientific) were used at 250 nM and 100 nM, respectively; NucView 488 caspase-3 substrate (Biotium) was used at 200 nM.

Manipulating cell growth rate to determine effects on drug sensitivity. RPE-1 or MCF 10A-H2B-mCherry cells were plated in 384-well plates using the Multidrop Combi Reagent Dispenser (Thermo Scientific) at 250 and 500 cells per well, respectively. To modulate the growth rate in RPE-1 cells, we induced expression of the $BRAF^{V600E}$ oncogene by treating cells with indicated doses of doxycycline using a D300 Digital Dispenser (Hewlett-Packard). To modulate the growth rate in MCF 10A-H2B-mCherry we serum-starved cells twice with DMEM/F12 medium supplemented with 0.1% bovine serum albumin and 1% penicillin–streptomycin. Medium changes and cell washing were performed using an EL406 Microplate Washer Dispenser (BioTek). Cells were treated with indicated doses of human epidermal growth factor (EGF, Peprotech) using a D300 Digital Dispenser. After 24 h the cells were treated with a dilution series of etoposide using a D300 Digital Dispenser. RPE-1 cells were stained and fixed for analysis at the time of drug treatment and after 72 h. MCF 10A-H2B-mCherry cells were imaged in an IncuCyte ZOOM live-cell imager (Essen Bioscience) starting at the time of EGF treatment, and drug sensitivity was evaluated 72 h after drug addition.

Evaluating drug-response metrics in MCF 10A and BT-20 over time. MCF10 A-H2B-mCherry and BT-20-H2B-mCherry cells were plated at 1,250 and 2,500 cells per well, respectively, in 384-well plates using the Multidrop Combi Reagent Dispenser (Thermo Scientific) and grown for 24 h. Cells were treated with a dilution series of the indicated drugs using a D300 Digital Dispenser (Hewlett-Packard) and imaged after drug addition in an Operetta High-Content Imaging System (PerkinElmer) equipped with a live-cell chamber over a period of 96 h. For these experiments, we used the following drugs:

- Etoposide, topoisomerase inhibitor
- Linsitinib, IGF1R inhibitor
- Omipalisib/GSK2126458, panPI3K/mTOR inhibitor
- PLX4720, B-RAF inhibitor
- Tanespimycin/17-AAG, HSP90 inhibitor

Evaluating drug sensitivity in MCF 10A spheroids over time. MCF10 A-H2B-mCherry cells were plated at 200 cells per well into ultralow attachment-coated, flat-bottom, 384-well plates (Corning) with the addition of 2.5% growth factor reduced basement membrane matrix Matrigel (Corning) to the growth medium. After 48 h, cells were treated with a dilution series of omipalisib using a D300 Digital Dispenser (Hewlett-Packard) and imaged in an IncuCyte ZOOM live-cell imager (Essen Bioscience) for an additional 96 h. Drug sensitivity was evaluated by computing GR values every 15 h over a 10–90 h time frame.

Evaluating drug sensitivity in breast cancer cells plated at different seeding densities. MCF 10A, Hs 578T, MDA-MB-231, MCF7, SK-BR-3, and BT-20 were plated at densities ranging from 156 to 5,000 cells per well in 384-well plates using the Multidrop Combi Reagent Dispenser (Thermo Scientific) and grown for 24 h. Cells were treated with a dilution series of the indicated drugs using a D300 Digital Dispenser (Hewlett-Packard). Cells were stained and fixed for analysis at the time of drug treatment and after 72 h of incubation with drug. For these experiments, we used the following drugs:

- Erlotinib, EGFR inhibitor
- Etoposide, topoisomerase inhibitor
- Lapatinib, EGFR/ErbB2 inhibitor
- Linsitinib, IGF1R inhibitor
- Methotrexate, dihydrofolate reductase inhibitor
- Omipalisib/GSK2126458, panPI3K/mTOR inhibitor
- Paclitaxel, target microtubules
- Palbociclib, CDK4/6 inhibitor
- PLX4720, B-RAF inhibitor
- TAE684, ALK inhibitor
- Tanespimycin/17-AAG, HSP90 inhibitor

Investigating density-dependent drug effects. MCF 10A-H2B-mCherry cells were plated at densities that ranged from 156 to 5,000 cells per well in 384-well plates using the Multidrop Combi Reagent Dispenser (Thermo Scientific) and grown for 24 h. Cells were treated with a dilution series of drugs using a D300 Digital Dispenser (Hewlett-Packard) and imaged after drug addition in an Operetta High-Content Imaging System (PerkinElmer) equipped with a live-cell chamber over a period of 72 h.

In the case of methotrexate and oligomycin, 1,250 cells were plated in 20–120 µL of medium per well, treated with a dilution series of drug, and imaged for 72 h.

doi:10.1038/nmeth.3853

In the case of linsitinib, cells were treated with a dilution series of linsitinib either with or without 10 μM batimastat using a D300 Digital Dispenser and imaged in an IncuCyte ZOOM live-cell imager (Essen Bioscience) for an additional 72 h.

In the case of paclitaxel, cells were treated with a dilution series of paclitaxel and 200 nM of NucView 488 caspase-3 substrate (Biotium) using a D300 Digital Dispenser (Hewlett-Packard) and imaged after drug in an IncuCyte ZOOM live-cell imager (Essen Bioscience) for an additional 72 h. For immunofluorescence experiments, cells were grown for 24 h and then treated with a dilution series of paclitaxel using a D300 Digital Dispenser (Hewlett-Packard) and incubated for 3, 6, 12, and 24 h. Cells were fixed for 30 min in 3% formaldehyde, permeabilized for 30 min in PBS with 0.3% Triton X-100 (Sigma-Aldrich), washed twice in PBS with 0.1% Tween 20 (Sigma-Aldrich; PBS-T), and blocked for 60 min with Odyssey blocking buffer (LI-COR Biosciences). Anti-active Caspase-3 antibody (BD Biosciences) was diluted 1:1,000 in Odyssey blocking buffer and incubated for 16 h at 4 °C. Cells were washed three times in PBS-T for 5 min and incubated with Alexa Fluor 488-conjugated goat anti-rabbit secondary antibody diluted 1:1,000 in Odyssey blocking buffer for 60 min at room. Cells were washed two times in PBS-T, washed once with PBS, stained for 30 min with whole cell stain (Thermo Fisher Scientific) and Hoechst (Thermo Fisher Scientific), and washed three times in PBS.

Fixed-cell endpoint assays. After drug treatment, cells were stained at the indicated timepoints with 2 μM Hoechst 33342 (Thermo Fisher Scientific) and LIVE/DEAD Far Red Dead Cell Stain (Thermo Fisher Scientific) for 30 min and fixed with 3% formaldehyde (Sigma-Aldrich) for 30 min. Fixed cells were imaged using an Operetta microscope and analyzed using the Columbus image data storage and analysis system (PerkinElmer).

Live-cell time course assays. Cells expressing H2B-mCherry were imaged at the indicated timepoints after drug treatment in an Operetta High-Content Imaging System (PerkinElmer) equipped with a live-cell chamber or an IncuCyte ZOOM live-cell imager. Dead cells were identified by counterstaining cells with YOYO-1 or TOTO-3 (Thermo Fisher Scientific), and apoptotic cells were identified with the NucView 488 caspase-3 substrate (Biotium). Live, dead, or apoptotic cell lines were identified using the Columbus image data storage and analysis system or the IncuCyte analysis software. Spheroid growth was estimated by measuring the sum of the spheroid area per well using IncuCyte analysis software.

mRNA analysis. mRNA analysis. Cells plated at different densities in 384-well plates were harvested at the indicated times, and RNA was extracted using the RNeasy mini kit (Qiagen). To ensure sufficient amounts of RNA, wells with a low number of cells were pooled. Libraries were prepared by the Broad Technology Labs (BTL), following the protocol for SCRB-Seq described in ref. 41. Transcripts were quantified by the BTL computational pipeline using Cuffquant v.2.2.1 (ref. 42). Analysis of the transcriptional data was performed in MATLAB using standard libraries and inhouse scripts. Gene set enrichment analysis was performed using the GSEA software v2.1.0 from the Broad Institute with the MSigDB v4.0 GO biological process set[43].

38. Nam, H.S. & Benezra, R. High levels of Id1 expression define B1 type adult neural stem cells. *Cell Stem Cell* **5**, 515–526 (2009).
39. Hockemeyer, D. *et al.* Efficient targeting of expressed and silent genes in human ESCs and iPSCs using zinc-finger nucleases. *Nat. Biotechnol.* **27**, 851–857 (2009).
40. Boehm, J.S. *et al.* Integrative genomic approaches identify IKBKE as a breast cancer oncogene. *Cell* **129**, 1065–1079 (2007).
41. Soumillon, M., Cacchiarelli, D., Semrau, S., van Oudenaarden, A. & Mikkelsen, T.S. Characterization of directed differentiation by high-throughput single-cell RNA-Seq. Preprint at http://biorxiv.org/content/early/2014/03/05/003236 (2014).
42. Trapnell, C. *et al.* Differential gene and transcript expression analysis of RNA-seq experiments with TopHat and Cufflinks. *Nat. Protoc.* **7**, 562–578 (2012).
43. Subramanian, A. *et al.* Gene set enrichment analysis: a knowledge-based approach for interpreting genome-wide expression profiles. *Proc. Natl. Acad. Sci. USA* **102**, 15545–15550 (2005).